Electronic Supplementary Information

Dual-mode fluorometric and colorimetric sensors based on carbon quantum dots-doped MIL-53(Fe) encapsulated in SiO_2 shells for fluoride detection

Yijun Mo[a], Ziyi Guo[a], Shenran Yu[a], Zihan Xu[a], Zetao Cai[a], Yudi Wang[a], Shi-Wen Lv[a,b,*], Yanqing Cong[a,b,*]

a. Zhejiang Key Laboratory of Solid Waste Pollution Control and Resource Utilization, School of Environmental Science and Engineering, Zhejiang Gongshang University, Hangzhou 310018, China

b. Tongxiang Institute of Artificial General Intelligence, Jiaxing 314000, China

*Corresponding author.

Mail to: No.18 Xuezheng Road, Hangzhou, 310018, China.

Email: yqcong@zjgsu.edu.cn (Yanqing Cong)

lvshiwen@zjgsu.edu.cn (Shi-Wen Lv)

Contents

Fig. S8. Effects of reaction temperature on the absorbance and fluorescence intensity changes of MIL-53(Fe)-CQDs@SiO_2 upon reaction with F^-.

Fig. S9. Effects of pH on the absorbance and fluorescence intensity changes of MIL-53(Fe)-CQDs@SiO_2 upon reaction with F^-.

Fig. S10. Effects of reaction time on the absorbance and fluorescence intensity changes of MIL-53(Fe)-CQDs@SiO_2 upon reaction with F^-.

Fig. S11. The TEM image of MIL-53(Fe)-CQDs@SiO_2 after reaction with F^-.

Fig. S12. The XRD of MIL-53(Fe) before and after reaction with F^-.

Text S1. Chemicals and reagents.

All chemicals and reagents used in this work are of analytical grade or higher. Citric Acid, formamide, N, N-dimethylformamide, $FeCl_3$•$6H_2O$, 1,4-benzenedicarboxylic acid (1,4-BDC), Tetraethyl orthosilicate (TEOS) and NH_3•H_2O were purchased from Macklin Co., Ltd. (Shanghai, China). Ethanol, dimethyl sulfoxide (DMSO), NaF and TMB were provided by Aladdin Chemistry Co. Ltd. (Shanghai, China).

Text S2. Electrochemical measurement.

With FTO glass sheet (1.0×1.0cm) as the working electrode, the saturated silver chloride electrode as reference electrode and Pt plate as counter electrode, measurement was carried out on a three-electrode system with CHI660E (Shanghai Chenhua, China) electrochemical workstation. The working electrode was prepared as follows: Firstly, 20 mg of catalyst were dispersed in 2 mL of anhydrous ethanol and 20 μL of Nafion (5%) solution and sonicated thoroughly to form a dispersion. Then evenly coat the dispersion onto FTO conductive glass, and finally heat treat at 60 ℃ for 30 min. Specifically, electrochemical impedance spectroscopy (EIS) was recorded with a 5 mV AC amplitude signal and frequency range of 105 Hz to 0.1 Hz. The cyclic voltammetry (CV) scans were employed for determining electrical double-layer capacitance of catalyst at different scan rates of 100, 200, 300, 400 and 500 mV/s.

Text S3. Characterization of the steady-state kinetics of samples.

The steady-state kinetics of samples were investigated by the varying concentration of TMB from 0.015 to 0.375 mM and the fixing concentration of H_2O_2 (0.375 mM), or vice versa. Subsequently, the maximum initial velocity (Vmax) and Michaelis-Menten constant (Km) were calculated by fitting the Lineweaver-Burk plot.

Text S4. Hydroxyl radical scavenging experiment.

To confirm the peroxidase-like catalytic mechanism, the production of •OH intermediates during the peroxidase-like reaction was monitored by EPR using DMPO as a spin trap. Typically, PBS buffer (pH 4.0, 0.1 M) containing 20 mM DMPO and 10 mM H_2O_2 were added in glass capillary tubes and sealed in the presence or absence of nanozymes (10 μg/mL). The EPR spectra were recorded after the above mixture reacted for 3 min at room temperature.

Text S5. Regulation of doping amount of CQDs and TEOS.

The incorporation amount of CQDs was modulated by varying the volume of the CQDs-containing DMF solution during the synthesis of MIL-53(Fe). As shown in Fig. S1a, with the increase in the doping amount of CQDs, the fluorescence intensity of MIL-53(Fe)-CQDs at 442 nm was significantly enhanced. Interestingly, an enhancement in absorbance at 652 nm was also observed with increasing CQDs incorporation Fig. S1b, indicating the crucial role of CQDs in boosting the peroxidase-like activity of MIL-53(Fe). Therefore, to obtain excellent fluorescent performance and peroxidase-like activity, the addition amount of the DMF solution containing carbon quantum dots (CQDs) was adjusted to 30 mL. Meanwhile, the thickness of SiO_2 was modulated by varying the amount of TEOS added. Fig. S 1a and b demonstrated the influence of different SiO_2 thickness levels on both the fluorescence property and peroxidase-like activity of MIL-53(Fe)-CQDs@SiO_2, with the increase in the coating amount of SiO_2, both of fluorescence property and peroxidase-like activity were inhibited. An addition amount of 0.8 mL TEOS was therefore selected to achieve a lower detection limit and a wider linear range. Fig. S showed the excitation and emission spectra of MIL-53(Fe)-CQDs@SiO_2.

Accordingly, the maximum fluorescence intensity was observed upon excitation at 360 nm, so 360 nm and 442 nm were chosen as the optimal excitation and emission wavelengths for subsequent measurements (Fig. S2).

Text S6. Conditions of dual-mode fluorometric and colorimetric detection.

For fluorometric analysis, 1 mL F^- standard solution (dissolved in acetate buffer) with different concentrations was added to 1 mL MIL-53(Fe)-CQDs@SiO_2 solution (1 mg/mL). For colorimetric analysis, 600 μL F^- standard solution with different concentrations was added to 1 mL acetate buffer, then adding 100 μL nanozymes solution (1 mg/mL). The reaction of SiO_2 and F^- was conducted at 55 ℃ for 40 min. After cooling to room temperature, 150 μL TMB solution and 150 μL H_2O_2 were added into the mixture for 5 min, and then the absorption of reaction system at 652 nm was determined. Furthermore, the fluorescent intensity of reaction system was directly measured without the addition of TMB and H_2O_2, and the excitation wavelength was set as 360 nm.

Text S7. Reaction of F^- with SiO_2 in acidic conditions

$$SiO_2+6HF\rightarrow 2H^++SiF_6^{2-}+2H_2O$$

Table S1. Comparison of the k_m values with other peroxidase mimetics.

Materials	Substance	k_m (mM)	Refs.
Fe_3O_4@MoS_2	H_2O_2	1.39	[1]
	TMB	0.25	
MIL-OH-D	H_2O_2	1.61	[2]
	TMB	1.35	
NH_2-MIL-88B	H_2O_2	0.17	[3]
	TMB	0.61	
Fe-MOF-GOx	H_2O_2	1.30	[4]
	TMB	2.60	
MIL-53(Fe, Al)	H_2O_2	0.11	[5]
	TMB	0.17	
MIL-53(Fe)-CQDs	H_2O_2	0.11	This work
	TMB	0.15	

Table S2. Comparison of other sensors reported for F^- determination.

Materials	Method	LOD μM	Linea range μM	Refs.
AgPt-Fe_3O_4@SiO_2	Colorimetry	13.73	500-2000	[6]
Fe-MOFs	Colorimetry	1	2-30	[7]
UiO 66-(NH_2)	Colorimetry	3.48	5-50	[8]
Sensor (AR)	Colorimetry	5.26	4.21-10530	[9]
SDS-Hp	Fluorimetry	37.8	53-526	[10]
CDs@Al^{3+}	Fluorimetry	7.99	150-1200	[11]
CDs@SiO_2	Fluorimetry	1	1-4000	[12]
CDs from wheat straw	Fluorimetry	49	00-1500	[13]
MIL-53(Fe)-CQDs@SiO_2	Colorimetry	0.71	2-15	This work
MIL-53(Fe)-CQDs@SiO_2	Colorimetry	9.51	20-300	This work
MIL-53(Fe)-CQDs@SiO_2	Fluorimetry	5.47	10-300	This work

Table S3. Storage stability test of MIL-53(Fe)-CQDs@SiO_2.

Materials	Tested (10μM) (Colorimetry)	Tested (200μM) (Colorimetry)	Tested (10μM) (Fluorometry)	Tested (200μM) (Fluorometry)
MIL-53(Fe)-CQDs@SiO_2 (day 1)	10.82±0.94 (n=3)	202.04±4.61 (n=3)	10.56±0.32 (n=3)	198.43±3.81 (n=3)
MIL-53(Fe)-CQDs@SiO_2 (day 3)	10.46±0.21 (n=3)	205.63±2.77 (n=3)	9.97±0.27 (n=3)	197.33±4.56 (n=3)
MIL-53(Fe)-CQDs@SiO_2 (day 5)	10.37±0.44 (n=3)	204.89±2.14 (n=3)	10.91±0.76 (n=3)	201.71±2.94 (n=3)

Table S4. Analytical performance for dual-mode fluorometric and colorimetric detection of F^- in Urban Groundwater and Fly Ash Stabilization Liquid.

Samples	Determined μM (Ion Chromatography)	Tested μM (Colorimetry)	Tested μM (Fluorometry)
Fly Ash Stabilization Liquid (a)	177.01	169.93±3.17 (n=3)	190.76±2.78 (n=3)
Fly Ash Stabilization Liquid (b)	255.64	258.96±3.66 (n=3)	267.88±4.03 (n=3)
Groundwater (a)	11.34	11.07±0.47 (n=3)	12.44±0.15 (n=3)
Groundwater (b)	13.57	12.91±0.33 (n=3)	14.08±0.23 (n=3)

References:

[1] F. Wei, X. Cui, Z. Wang, C. Dong, J. Li, X. Han, Recoverable peroxidase-like Fe_3O_4@MoS_2-Ag nanozyme with enhanced antibacterial ability, Chemical Engineering Journal, 408 (2021) 127240.

[2] W. Xu, L. Jiao, H. Yan, Y. Wu, L. Chen, W. Gu, D. Du, Y. Lin, C. Zhu, Glucose oxidase-integrated metal–organic framework hybrids as biomimetic cascade nanozymes for ultrasensitive glucose biosensing, ACS Applied Materials & Interfaces, 11 (2019) 22096-22101.

[3] Z. Lu, Y. Dang, C. Dai, Y. Zhang, P. Zou, H. Du, Y. Zhang, M. Sun, H. Rao, Y. Wang, Hollow MnFeO oxide derived from MOF@MOF with multiple enzyme-like activities for multifunction colorimetric assay of biomolecules and Hg^{2+}, Journal of Hazardous Materials, 403 (2021) 123979.

[4] Z. Li, F. Meng, R. Li, Y. Fang, Y. Cui, Y. Qin, M. Zhang, Amino−functionalized Fe(III)−Based MOF for the high−efficiency extraction and ultrasensitive colorimetric detection of tetracycline, Biosensors and Bioelectronics, 234 (2023) 115294.

[5] J. Tang, Z. Gao, L. Xu, Q. Zhao, T. Hu, Y. Luo, J. Dou, Y. Bai, L. Xia, K. Du, Smartphone-assisted colorimetric biosensor for the rapid visual detection of natural antioxidants in food samples, Food Chemistry, 462 (2025) 141026.

[6] Z. Qiu, W. Duan, S. Cao, T. Zeng, T. Zhao, J. Huang, X. Lu, J. Zeng, Highly specific colorimetric probe for fluoride by triggering the intrinsic catalytic activity of a AgPt–Fe_3O_4 hybrid nanozyme encapsulated in SiO_2 shells, Environmental Science & Technology, 56 (2022) 1713-1723.

[7] D. Hou, Y. You, X. Wu, C. Li, S. Wu, C. Zhang, Y. Xian, A nanosized metal–organic framework for visual detection of fluoride ions with smartphone via colorimetric test kit, Sensors and Actuators B: Chemical, 332 (2021) 129508.

[8] Q. Li, H. Chen, S. You, Z. Lin, Z. Chen, F. Huang, B. Qiu, Colorimetric and fluorescent dual-modality sensing platform based on UiO-66 for fluorion detection, Microchemical Journal, 186 (2023) 108318.

[9] H. Javadi, F. F. Kooshki, E. Saleh, G. Golchin, R. Sedghi, A facile synthesis of a novel polymer-based nanocomposite as colorimetric response sensor for fluoride ion detection in real-life complex mediums, Journal of Environmental Chemical

Engineering 12.6 (2024): 114098.

[10] A. Halder, S. Singh, A. Adhikari, P. Singh, P.K. Sarkar, U. Pal, R. Ghosh, D. Shikha, Y.S. Solanki, M. Agarwal, A.B. Gupta, R. Chakraborty, T. Saha-Dasgupta, R. Das, S.K. Pal, Selective and fast responsive sensitized micelle for detection of fluoride level in drinking water, ACS Sustainable Chemistry & Engineering, 7 (2019) 16355-16363.

[11] L. Yan, B. Zhang, Z. Zong, W. Zhou, S. Shuang, L. Shi, Artificial intelligence-integrated smartphone-based handheld detection of fluoride ion by Al^{3+}-triggered aggregation-induced red-emssion enhanced carbon dots, Journal of Colloid and Interface Science, 651 (2023) 59-67.

[12] M.-X. Liu, X.-B. Chen, W.-Y. Liu, J.-H. Wang, Y.-L. Yu, S. Chen, Phosphorescence approach based on silica protected carbon dots for autofluorescence interference-free and highly selective detection of fluoride, Analytica Chimica Acta, 1287 (2024) 342102.

[13] S. Liu, Z. Liu, Q. Li, Xia, H. Xia, W. Yang, R. Wang, Y. Li, H. Zhao, B. Tian, Facile synthesis of carbon dots from wheat straw for colorimetric and fluorescent detection of fluoride and cellular imaging, Spectrochimica Acta Part A: Molecular and Biomolecular Spectroscopy 246 (2021): 118964.

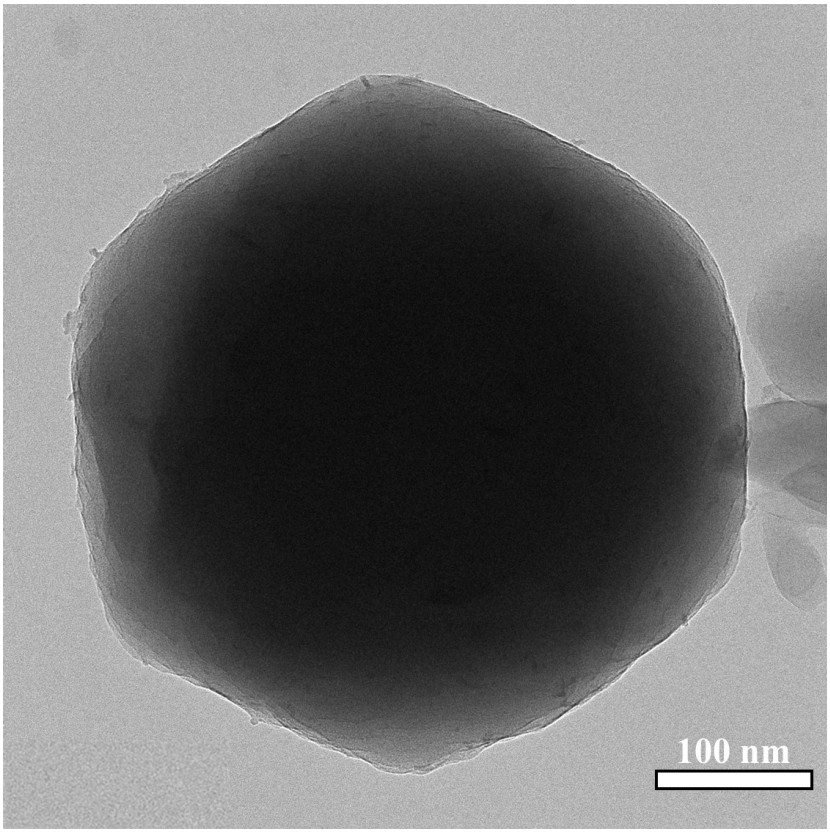

Fig. S1. Typical TEM image of MIL-53(Fe).

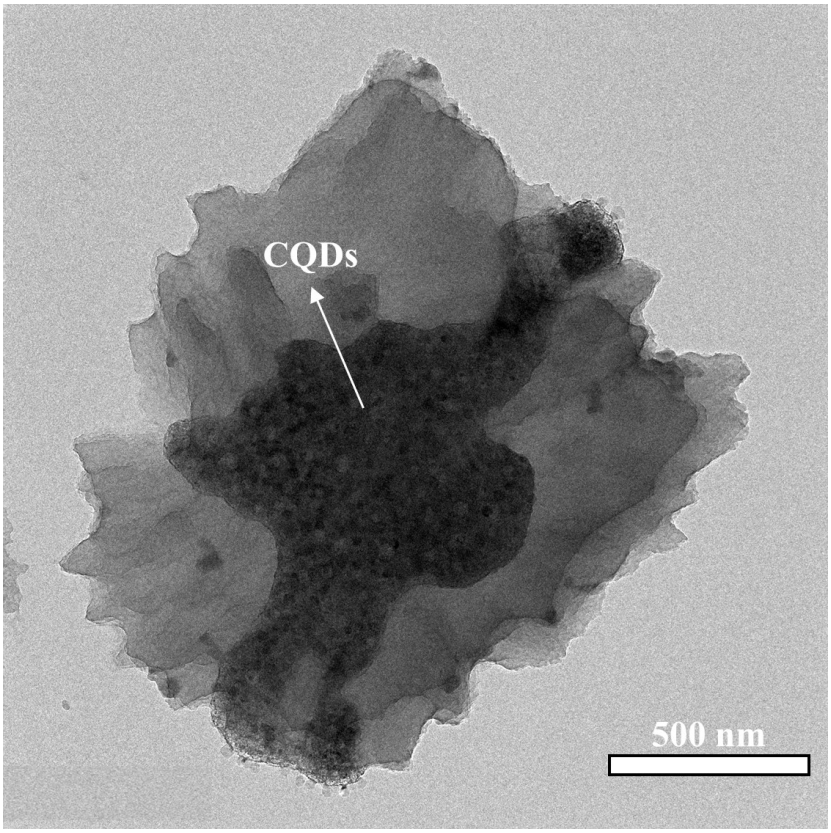

Fig. S2. Typical TEM image of MIL-53(Fe)-CQDs.

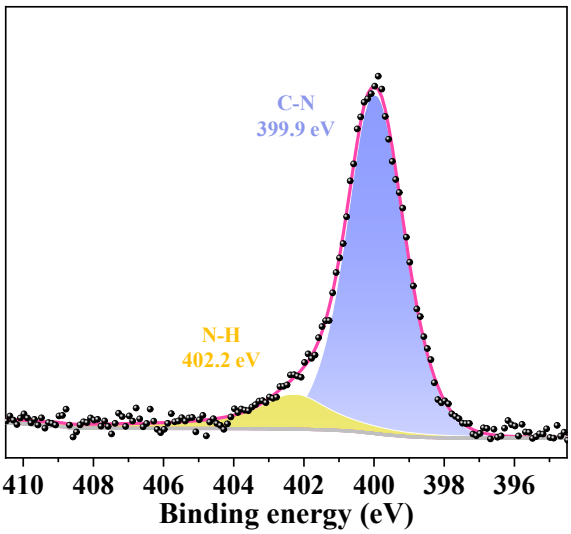

Fig. S3. The high-resolution XPS profiles of MIL-53(Fe)-CQDs@SiO_2: N 1s.

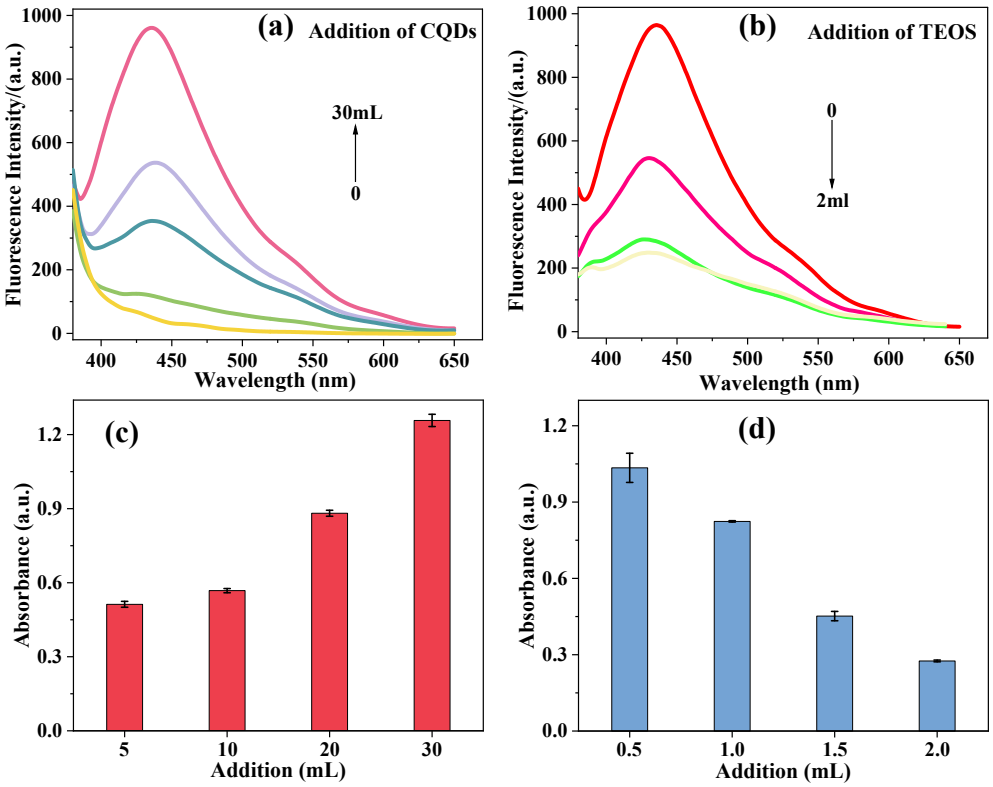

Fig. S4. Optimization of the CQDs loading and the SiO_2 thickness. Fluorescence emission spectra of sample with different amounts of (a) CQDs, (b) TEOS. Changed absorbance at 652 nm of sample with different amounts of (c) CQDs, (d) TEOS.

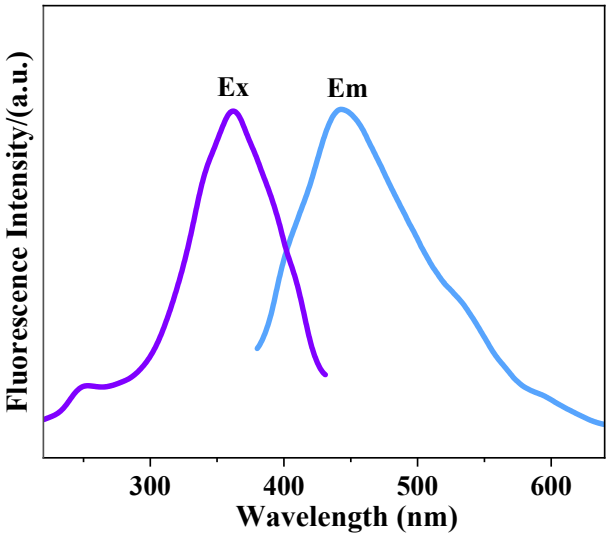

Fig. S5. Fluorescence excitation and emission spectra of MIL-53(Fe)-CQDs@SiO_2.

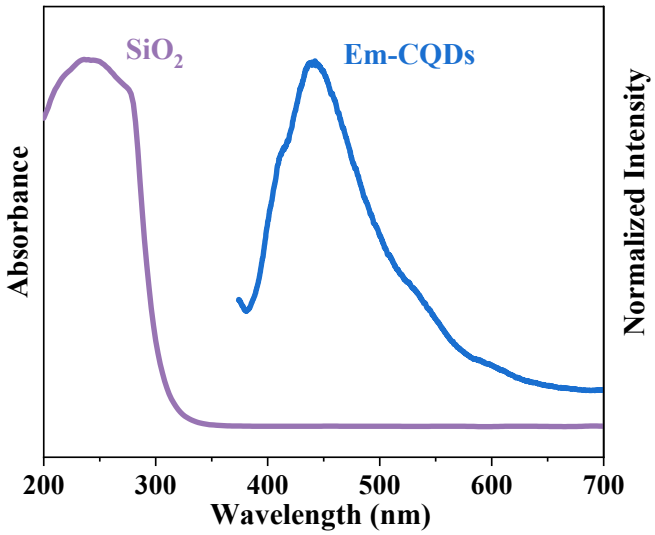

Fig. S6. Fluorescence emission spectra of CQDs and UV-Vis absorption spectroscopy of SiO_2.

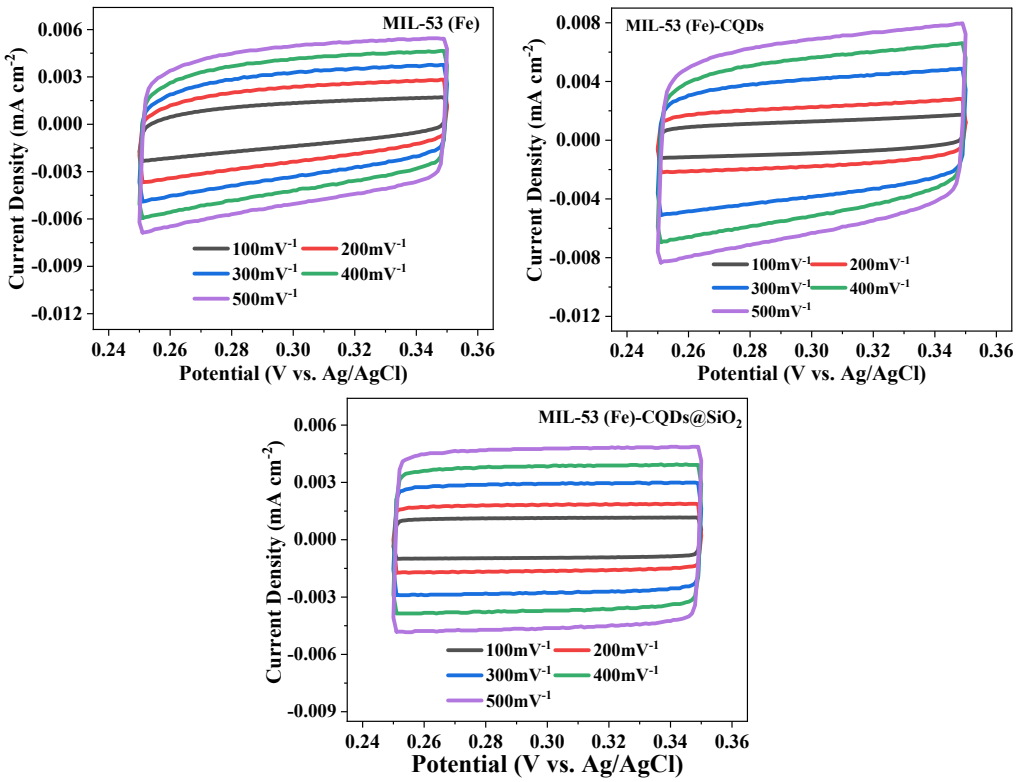

Fig. S7. CV curves of samples.

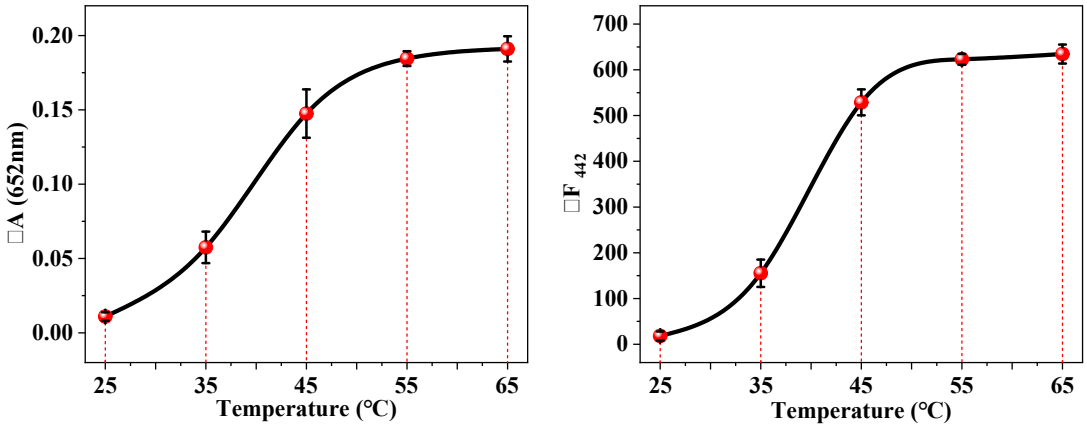

Fig. S8. Effects of reaction temperature on the absorbance and fluorescence intensity changes of MIL-53(Fe)-CQDs@SiO_2 upon reaction with F^-.

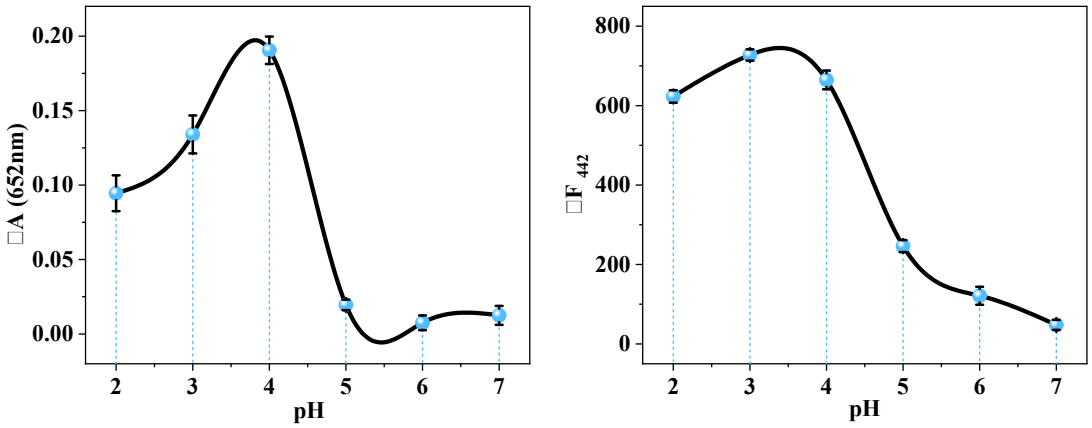

Fig. S9. Effects of pH on the absorbance and fluorescence intensity changes of MIL-53(Fe)-CQDs@SiO_2 upon reaction with F^-.

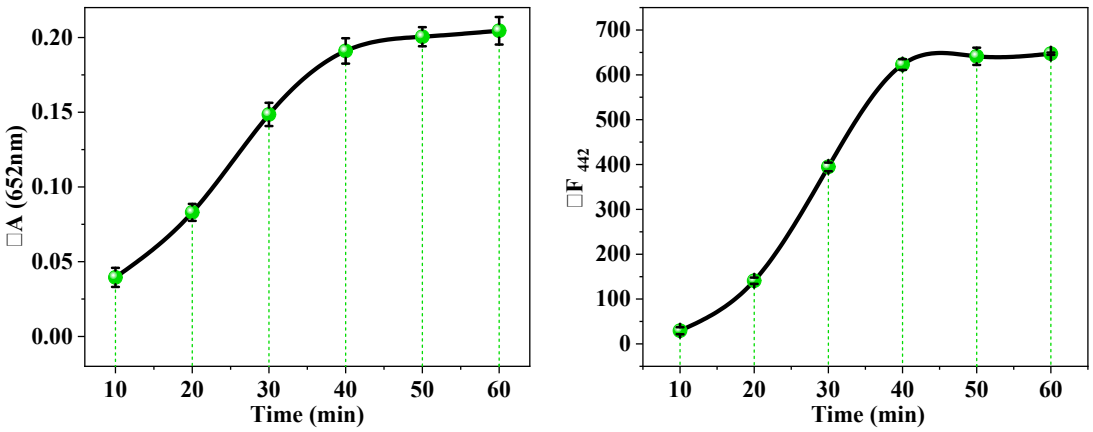

Fig. S10. Effects of reaction time on the absorbance and fluorescence intensity changes of MIL-53(Fe)-CQDs@SiO_2 upon reaction with F^-.

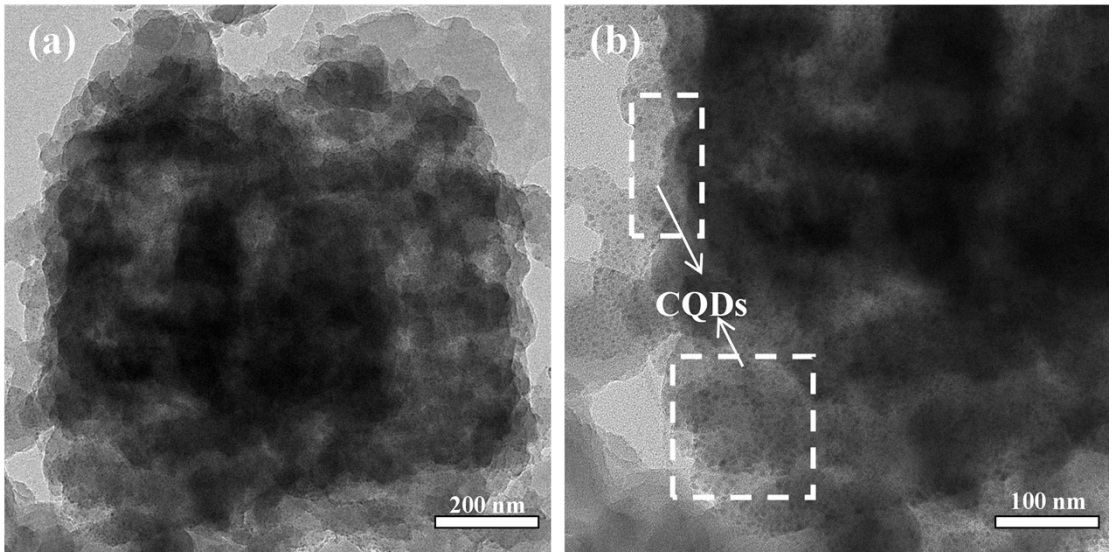

Fig. S11. The TEM image of MIL-53(Fe)-CQDs@SiO_2 after reaction with F^-.

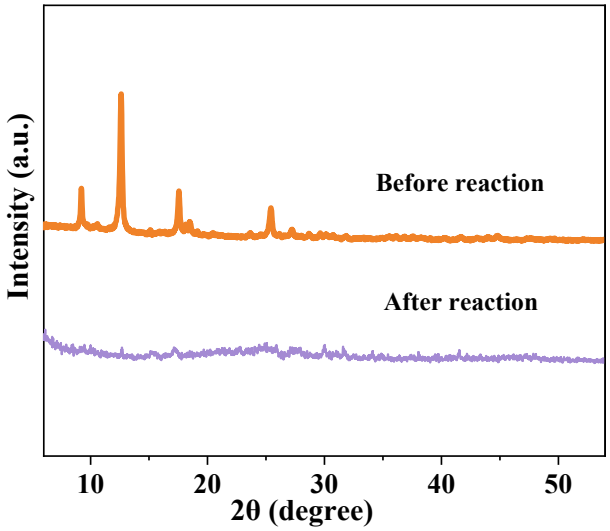

Fig. S12. The XRD of MIL-53(Fe) before and after reaction with F^-.